Stochastic Modeling and Applications
Vol.21, No. 1(June, 2017)

HEAT AND MASS TRANSFER OF NANOFLUID IN A VERTICALLY RECIPROCATING DISK

S. PRASANNA RANI

ABSTRACT. In the current research work, a detailed analysis of the flow, heat and mass transfer of a fluid over a vertically reciprocating disk using the von Kármán flow model is conducted. The influence of the Darcy-Forchheimer porous medium, vertical reciprocation, heat source/sink and homogeneous-heterogeneous reaction on the flow, thermal and concentration fields is studied. The similarity transformations are used to transform the partial differential equation into an ordinary differential equation, which is numerically solved using the Runge-Kutta-Fehlberg fourth-fifth order method. The radial and tangential velocities decrease with increasing Darcy-Forchheimer and porous-medium parameters, whereas the reciprocation parameter causes a reduction in the concentration and temperature profiles, but an increase in tangential velocity. Temperature rises with increasing heat source/sink parameter, while the concentration drops with an increase in the homogeneous reaction parameter. Moreover, response surface methodology is adopted to analyse the heat transfer process. The results might help design and optimize energy-conversion devices incorporating porous media and reactive fluid flows, as well as chemical reactors, thermal processing equipment and filtration systems.

1. Nomenclature

Symbols	Descriptions	Symbols	Descriptions
$\omega(t)$	Angular speed	c	Arbitrary constant
$T_d(t)$	Disk surface temperature	a	Wall temperature parameter
T_∞	Ambient temperature	(u, v, w)	Velocity component
δ	Wall permeability parameter	(r, ϕ, z)	Cylindrical coordinates
$b(t)$	Vertical position	(U, V, W)	Dimensionless velocity profile
S	Reciprocating parameter	Pr	Prandtl number
Sc	Schmit number	θ	Temperature profile
ϖ_d and ϖ_f	Rotation of disk and fluid	ρ	Density
D_A and D_B	Diffusion coefficient	A and B	Chemical species
ρC_p	Specific heat	ν	Kinematic viscosity
μ	Dynamic viscosity	k	Thermal conductivity
Φ	Volume fraction	K^*	Porous media parameter
K_1	Homogenous parameter	F_1	Darcy-Forchheimer

2000 *Mathematics Subject Classification.* 76D05, 76R50, 76R99.
Key words and phrases. Reciprocating disk; Tetra hybrid nanofluid; Heat source/sink; Homogeneous-heterogeneous reaction; Response surface method.

2. Introduction

A reciprocating disk is a disk that moves upward and downward along a specified axis, causing unsteady flow within the fluid. The disk's periodic motion creates temporal variations in velocity, wall shear and temperature profiles, resulting in a flow significantly different from that over a stationary or continuously rotating disk. Reciprocating disk configurations are applicable to mechanical actuators, piston-like devices, oscillatory cooling systems, lubrication processes and thermal management equipment. Their analysis can help to understand the influence of periodic surface motion on fluid flow and heat transfer properties. Komoda et al. [8] exemplified the performance of mixing by a reciprocating disk in a cylindrical vessel. Komoda et al. [9] studied the laminar flow of fluid due to a reciprocating disk in a cylindrical vessel. Hirata et al. [5] investigated the mixing performance of a reciprocating disk in a cylindrical vessel.

Tetra-hybrid nanofluids are a new generation of hybrid nanofluids, formed by dispersing four types of nanoparticles into a conventional base fluid. Multiple nanoparticles can be incorporated into the base fluid simultaneously, which may significantly alter effective thermophysical properties, such as thermal conductivity. The properties of the constituent nanoparticles make it more flexible to control the heat transfer process than with mono-, hybrid, or ternary nanofluids. Tetra-hybrid nanofluids are therefore interesting for use in high-performance heat exchangers, electronic cooling, solar thermal systems, energy conversion equipment, etc., as a result of improved thermal management and heat transfer. Sheikholeslami et al. [14] studied the nanofluid flow between two horizontal plates with magnetohydrodynamic effect. Akbari et al. [1] analysed nanofluid flow in a three-dimensional rectangular microchannel. Mohammed et al. [10] addressed the flow and heat transfer of nanofluid in microchannels.

The heat source/sink parameter represents an internal heat source or sink, such as heating or cooling the fluid. A heat source is a positive energy source that tends to raise the fluid's energy content and generally increases its temperature, while a heat sink is a negative energy source that tends to lower the fluid's energy content. The thermal behaviour of the system can be controlled beyond the imposed boundary conditions when the heat source/sink is included in the governing energy equation. Electronic cooling, chemical reactors, nuclear systems, polymer processing, solar thermal systems and industrial heat-management processes are all related to heat generation or absorption. Deng [3] studied the natural convection in a two-dimensional square cavity with heat source/sink effect. Using the heat source/sink effect, Qasim [12] depicted the flow of Jeffrey fluid with heat source/sink over a stretching sheet. Pal [11] analysed the thermal radiation and heat source/sink effect on a fluid flow over a permeable stretching surface.

Homogeneous-heterogeneous reactions refer to a combination of fluid-volume and reactive-surface reactions. The homogeneous reaction is distributed throughout the fluid and affects the concentration field, while the heterogeneous reaction occurs at the boundary and can either consume or produce chemical species. It is important to consider both mechanisms together, as describing reactive flows more realistically requires accounting for both processes in concert rather than separately. These coupled reactions are significant in catalytic processes, combustion systems, chemical reactors, pollutant removal, surface coating and industrial processes with reactive fluid-solid interfaces. Their interaction directly impacts the distribution of concentration and mass transfer. Kameswaran et al. [6] examined the heat transfer and flow of nanofluid in the presence of homogeneous-heterogeneous chemical reaction. Shaw et al. [13] probed the heat transfer and flow of micropolar fluid past a stretching sheet with homogeneous-heterogeneous chemical reaction. Hayat et al. [4] investigated the heat transfer and Powell-Eyring fluid flow with homogeneous-heterogeneous chemical reaction effects.

Response surface methodology (RSM) is a statistical and mathematical approach for exploring the relationship between multiple input parameters and a desired response. It builds an empirical model from a set of systematically designed numerical or experimental observations and can later be used to find the optimal operating conditions. RSM is very helpful when multiple parameters affect a response simultaneously, as it can reduce the number of simulations required and provide information on parameter effects and interactions. In heat transfer studies, RSM can be used to optimize quantities such as the Nusselt number and to identify parameter combinations that yield better thermal performance. Bezerra et al. [2] addressed RSM as an optimisation tool for analytical chemistry. Khuri and Mukhopadhyay [7] elucidated the various stages of development of RSM. Trinh and Kang [15] probed the optimization of coagulation tests using RSM.

The uniqueness of the present study lies in the detailed study of von Karman flow over a vertically reciprocating rotating disk using a tetra-hybrid nanofluid in a porous medium. In the present mathematical model, unique aspects such as Darcy-Forchheimer resistance, heat source/sink and homogeneous–heterogeneous chemical reaction are considered to investigate the momentum, thermal, and mass transport behaviours. The use of four different nanoparticles in the base fluid improves the thermophysical properties. It provides an extended view of the performance of heat transfer compared to the traditional nanofluids and hybrid nanofluids. The simultaneous use of both disk rotation and vertical reciprocation also provides a practical approach to investigating transport behaviours in rotating and moving systems. After that, the governing equations are transformed into a nonlinear system of ordinary differential equations (ODEs) via appropriate similarity transformations, which are solved numerically by the Runge-Kutta-Fehlberg fourth-fifth order (RKF-45) method. Moreover, RSM is used to analyze the effects of the parameters and find their interaction on the temperature profile.

3. Mathematical analysis

For the current study, the axisymmetric von Karman flow of a tetra-hybrid nanofluid past an infinitely reciprocating rotating disk is discussed. The disk is placed within a porous medium that is spinning at an angular speed $\omega(t)$ along with moving vertically. In this case, the fluid exists on the upper side of the disk, and cylindrical coordinates (r, ϕ, z) are used, which are the radial, azimuthal and axial coordinates, respectively. Their velocity components are given by u, v, and w, respectively. As far as the fluid away from the disk remains static $(\Omega = 0)$ but the disk is spinning $(\omega \neq 0)$, this setup becomes von Karman flow. The disk is located at the coordinate $z = b(t)$, where $b(t)$ represents its current vertical position. This means that the vertical speed of the disk is $w = \frac{\partial b(t)}{\partial t}$. The disk also moves with an angular speed of $\omega(t)$ and hence the fluid flow over the reciprocating disk. The tetra-hybrid nanofluids are obtained by dispersion of four kinds of nanoparticles in the base fluid and the effective thermophysical properties of these suspensions are used in the governing equation. The nanofluid far from the disk is maintained at a constant ambient temperature T_∞, whereas the disk surface temperature $T_d(t)$ is assumed to vary with time due to the vertical motion of the disk. It is defined as:

$$T_d\left(t\right) = T_\infty + \frac{c}{\left(b\left(t\right)\right)^{2a}}.$$

Where c is an arbitrary constant and a is the wall temperature parameter. The case $a = 0$ corresponds to a constant surface temperature, while $a \neq 0$ represents a time-dependent thermal boundary condition influenced by the disk motion. The porous medium resistance is considered in the momentum equations through Darcy and Forchheimer resistances. The thermal phenomena are modelled via the energy equation, considering the presence of a heat source/sink and the species transport equations by including homogeneous reactions in the fluid and heterogeneous reactions on the disk surface.

The governing equations are as follows:

$$\frac{\partial u}{\partial r} + \frac{\partial w}{\partial z} + \frac{u}{r} = 0, \tag{1}$$

$$\left.\begin{aligned} &\frac{\partial u}{\partial t} + \left[u\frac{\partial u}{\partial r} + w\frac{\partial u}{\partial z} - \frac{v^2}{r}\right] - 2\Omega v = \frac{\mu_{Thnf}}{\rho_{Thnf}}\left[\frac{\partial^2 u}{\partial z^2} + \frac{\partial^2 u}{\partial r^2} - \frac{u}{r^2} + \frac{1}{r}\frac{\partial u}{\partial r}\right] \\ &-\frac{1}{\rho_{Thnf}}\frac{\partial p}{\partial r} - \frac{\mu_{Thnf}}{\rho_{Thnf}K}u - F^* u^2, \end{aligned}\right\} \tag{2}$$

$$\left.\begin{aligned} &\frac{\partial v}{\partial t} + \left[u\frac{\partial v}{\partial r} + w\frac{\partial v}{\partial z} - \frac{uv}{r}\right] + 2\Omega u = \frac{\mu_{Thnf}}{\rho_{Thnf}}\left[\frac{\partial^2 v}{\partial z^2} + \frac{\partial^2 v}{\partial r^2} - \frac{v}{r^2} + \frac{1}{r}\frac{\partial v}{\partial r}\right] \\ &-\frac{\mu_{Thnf}}{\rho_{Thnf}K}v - F^* v^2, \end{aligned}\right\} \tag{3}$$

$$\frac{\partial w}{\partial t} + \left[u\frac{\partial w}{\partial r} + w\frac{\partial w}{\partial z}\right] + \frac{1}{\rho_{Thnf}}\frac{\partial p}{\partial z} = \frac{\mu_{Thnf}}{\rho_{Thnf}}\left[\frac{\partial^2 w}{\partial z^2} + \frac{\partial^2 w}{\partial r^2} + \frac{1}{r}\frac{\partial w}{\partial r}\right], \tag{4}$$

Energy equation

$$(\rho C_p)_{Thnf}\left[\frac{\partial T}{\partial t} + u\frac{\partial T}{\partial r} + w\frac{\partial T}{\partial z}\right] = k_{Thnf}\left[\frac{\partial^2 T}{\partial z^2} + \frac{\partial^2 T}{\partial r^2} + \frac{1}{r}\frac{\partial T}{\partial r}\right] + Q_0\left(T - T_\infty\right). \tag{5}$$

Homogeneous-heterogeneous reaction

$$\frac{\partial a}{\partial t} + u\frac{\partial a}{\partial r} + w\frac{\partial a}{\partial z} = D_A\left[\frac{\partial^2 a}{\partial z^2} + \frac{\partial^2 a}{\partial r^2} + \frac{1}{r}\frac{\partial a}{\partial r}\right] - k_c a b^2, \tag{6}$$

$$\frac{\partial b}{\partial t} + u\frac{\partial b}{\partial r} + w\frac{\partial b}{\partial z} = D_B\left[\frac{\partial^2 b}{\partial z^2} + \frac{\partial^2 b}{\partial r^2} + \frac{1}{r}\frac{\partial b}{\partial r}\right] + k_c a b^2. \tag{7}$$

The corresponding boundary conditions are

$$\left.\begin{aligned} &u = 0,\ v = \omega r,\ w = \delta\frac{\partial b(t)}{\partial t},\ T = T_d,\ D_A\frac{\partial a}{\partial z} = k_s a,\ D_B\frac{\partial b}{\partial z} = -k_s a \ \text{ at } z = b\left(t\right), \\ &u = 0,\ v = \Omega r,\ T = T_\infty,\ a = a_0,\ b = 0 \ \text{ as } z \to \infty. \end{aligned}\right\} \tag{8}$$

The wall permeability parameter δ is introduced to characterize the mass transfer through the disk surface and to represent different physical wall conditions. Specifically, $\delta = 1$ corresponds to an impermeable surface with no mass flux across the wall. When $\delta > 1$, the condition represents wall injection (blowing), where fluid is introduced into the boundary layer, leading to a thickening of the velocity and thermal boundary layers. Conversely, $\delta < 1$ corresponds to wall suction, where fluid is withdrawn from the surface, resulting in a thinning of the boundary layer and enhanced heat transfer characteristics.

The appropriate similarity transformations are as follows:

$$
\left.\begin{array}{l}
u = \frac{r\nu_f U}{b^2(t)},\ v = \frac{r\nu_f V}{b^2(t)},\ w = \frac{\nu_f W}{b(t)},\ p = \frac{\rho_f \nu_f P}{b^2(t)}, \\
T = T_\infty + (T_d - T_\infty)\,\theta,\ a = a_0\chi,\ b = a_0\phi,\ \eta = \frac{z}{b(t)} - 1.
\end{array}\right\} \tag{9}
$$

Using Eq. (9), the Eqs. (1)-(5) are reduced and obtained as follows:

$$
2U + W' = 0, \tag{10}
$$

$$
\left.\begin{array}{l}
U'' - A_1 A_2 \left[U^2 - V^2 + U'W - 2\varpi_f V - S\left(\frac{(\eta+1)}{2}U' + U\right)\right] \\
-\frac{1}{A_1 A_2}\varpi_d K^* U - F_1 U^2 = 0,
\end{array}\right\} \tag{11}
$$

$$
\left.\begin{array}{l}
V'' - A_1 A_2 \left[2UV + WV' + 2\varpi_f U - S\left(\frac{(\eta+1)}{2}V' + V\right)\right] \\
-\frac{1}{A_1 A_2}\varpi_d K^* V - F_1 V^2 = 0,
\end{array}\right\} \tag{12}
$$

$$
P' - \frac{1}{A_2}\left[W''\right] - A_1 \frac{S}{2}\left[(\eta+1)\,W' + W\right] + A_1 W W' = 0, \tag{13}
$$

$$
A_3\theta'' + A_4 \Pr\left[\frac{S}{2}(\eta+1)\,\theta' + aS\theta - W\theta'\right] + Q\theta = 0. \tag{14}
$$

$$
\chi'' + \frac{(\eta+1)}{2} Sc\, S\chi' - ScW\chi' - ScK_1\chi\phi^2 = 0, \tag{15}
$$

$$
\phi'' + \frac{(\eta+1)}{2}\xi Sc\, S\phi' - \xi ScW\phi' + \xi ScK_1\chi\phi^2 = 0. \tag{16}
$$

Reduced boundary conditions are

$$
\left.\begin{array}{l}
U = 0,\ V = \varpi_d,\ W = \delta\frac{S}{2},\ \theta = 1,\ \chi' = K_2\chi,\ \phi' = -K_2\xi\chi \quad at \quad \eta = 0 \\
U = 0,\ V = \varpi_f,\ \theta = 0,\ \chi = 1,\ \phi = 0 \qquad as \quad \eta \to \infty.
\end{array}\right\} \tag{17}
$$

The dimensionless parameters obtained are as follows:

$$
\left.\begin{array}{l}
S = \frac{2b(t)\frac{\partial b(t)}{\partial t}}{\nu_f},\ Pr = \frac{(\rho C_p)_f \nu_f}{k_f},\ \varpi_f = \frac{\Omega(t) b^2(t)}{\nu_f},\ \xi = \frac{D_A}{D_B}, \\
F_1 = F^* r,\ \varpi_d = \frac{\omega(t) b^2(t)}{\nu_f},\ K^* = \frac{\nu_f}{K\omega(t)},\ Sc = \frac{\nu_f}{D_A},\ K_1 = \frac{k_c b^2(t) a_0^2}{\nu_f} \\
K_2 = \frac{k_s b(t)}{D_A},\ A_1 = \frac{\rho_{Thnf}}{\rho_f},\ A_2 = \frac{\mu_f}{\mu_{Thnf}},\ A_3 = \frac{k_{Thnf}}{k_f},\ A_4 = \frac{(\rho C_p)_{Thnf}}{(\rho C_p)_f}.
\end{array}\right\} \tag{18}
$$

Here, S represents the vertical reciprocation of the disk, which governs the upward or downward motion of the surface. A positive value ($S > 0$) corresponds to the upward motion of the disk, while a negative value ($S < 0$) indicates downward movement. This parameter also reflects the effective expansion or contraction of the flow domain. It is closely associated with wall transpiration effects, thereby influencing the development of the velocity and thermal boundary layers. ϖ_d and ϖ_f denote the rotation of the disk and the nanofluid, respectively.

In this case, it is assumed that chemical species A and B have similar diffusion coefficients. This leads to the additional assumption that the diffusion coefficients D_A and D_B are identical, i.e., $\xi = 1$, and hence

$$\chi(\eta) + \phi(\eta) = 1. \tag{19}$$

Thus Eqns. (15) and (16) become

$$\chi'' + \frac{(\eta+1)}{2} Sc\, S\chi' - ScW\chi' - ScK_1\chi(1-\chi)^2 = 0, \tag{20}$$

With the boundary conditions

$$\left.\begin{array}{l} \chi' = K_2\chi \ at\ \eta = 0, \\ \chi = 1 \ \ as\ \ \eta \to \infty. \end{array}\right\} \tag{21}$$

4. Methodology

In the current analysis, the RKF-45 scheme along with the shooting algorithm is utilized in order to solve the converted nonlinear ODEs numerically. RKF-45 scheme is a highly efficient numerical method used for solving nonlinear and coupled ODE systems in fluid mechanics and heat transfer problems. The RKF-45 scheme includes embedded fourth- and fifth-order Runge-Kutta formulas, which automatically calculate the step size. The ability to adjust the step size ensures high accuracy of the numerical computations without unnecessary use of computational time where the solution varies slowly. The shooting method transforms the boundary value problem into an equivalent initial value problem by determining unknown initial conditions and correcting them to satisfy prescribed boundary conditions. The RKF-45 shooting method proves to be particularly suitable for the present problem due to the significant nonlinearity of coupled velocity and temperature profiles and the complexity of the boundary conditions. The governing equations are solved numerically by applying the RKF-45 shooting method. The following assumptions are made for the numerical solution:

$$\left.\begin{array}{l} \lambda_1 = U(\eta), \lambda_2 = U'(\eta), \lambda_3 = V(\eta), \lambda_4 = V'(\eta), \lambda_5 = W(\eta), \\ \lambda_6 = W'(\eta), \lambda_7 = \theta(\eta), \lambda_8 = \theta'(\eta), \lambda_9 = \chi(\eta), \lambda_6 = \chi'(\eta). \end{array}\right\} \tag{22}$$

Using the above equations, the reduced equations become,

$$\lambda_2' = F_1{\lambda_2}^2 + \frac{1}{A_1A_2}\varpi_d K^*\lambda_1 + A_1A_2\left[{\lambda_1}^2 - {\lambda_3}^2 + \lambda_2\lambda_5 - 2\varpi_f\lambda_3 - S\left(\frac{(\eta+1)}{2}\lambda_2 + \lambda_1\right)\right], \tag{23}$$

$$\lambda_4' = F_1{\lambda_3}^2 + \frac{1}{A_1A_2}\varpi_d K^*\lambda_3 + A_1A_2\left[2\lambda_1\lambda_3 + \lambda_5\lambda_4 + 2\varpi_f\lambda_1 - S\left(\frac{(\eta+1)}{2}\lambda_4 + \lambda_3\right)\right], \tag{24}$$

$$\lambda_6' = A_2\left[P' - A_1\frac{S}{2}\left[(\eta+1)\lambda_6 + \lambda_5\right] + A_1\lambda_5\lambda_6\right], \tag{25}$$

$$\lambda_8' = -\frac{1}{A_3}\left\{A_4 \Pr\left[\frac{S}{2}(\eta+1)\lambda_8 + aS\lambda_7 - \lambda_5\lambda_8\right] + Q\lambda_7\right\}. \tag{26}$$

$$\lambda_{10}' = -\frac{(\eta+1)}{2} Sc\, S\lambda_{10} + ScW\lambda_{10} + ScK_1\lambda_9 \left(1-\lambda_9\right)^2, \tag{27}$$

The boundary conditions are as follows,

$$\left.\begin{array}{l} \lambda_1 = 0,\ \lambda_3 = \varpi_d,\ \lambda_5 = \delta\frac{S}{2},\ \lambda_7 = 1,\ \lambda_{10} = K_2\lambda_9, \quad \text{at} \quad \eta = 0 \\ \lambda_1 = 0,\ \lambda_3 = \varpi_f,\ \lambda_5 = 0,\ \lambda_9 = 1, \qquad \text{as} \quad \eta \to \infty. \end{array}\right\} \tag{28}$$

The thermophysical properties of the tetra-hybrid nanofluid are given as,
Dynamic viscosity:

$$\mu_{Thnf} = \frac{\mu_f}{\left(1-\Phi_1\right)^{2.5}\left(1-\Phi_2\right)^{2.5}\left(1-\Phi_3\right)^{2.5}\left(1-\Phi_4\right)^{2.5}}. \tag{29}$$

Density:

$$\rho_{Thnf} = \left[\left(1-\Phi_1\right)\left\{\left(1-\Phi_2\right)\left(1-\Phi_3\right)\left[\left(1-\Phi_4\right)\Phi_f + \rho_4\Phi_4\right] + \rho_3\Phi_3 + \rho_2\Phi_2\right\} + \rho_1\Phi_1\right]. \tag{30}$$

Specific heat:

$$(\rho C_p)_{Thnf} = \left(1-\Phi_1\right)\left\{\begin{array}{l} \left(1-\Phi_2\right)\left(1-\Phi_3\right)\left[\begin{array}{l} \left(1-\Phi_4\right)(\rho C_p)_f \\ +(\rho C_p)_{s4}\Phi_4 \end{array}\right] \\ +(\rho C_p)_{s3}\Phi_3 + (\rho C_p)_{s2}\Phi_2 \end{array}\right\} + (\rho C_p)_{s1}\Phi_1. \tag{31}$$

Thermal conductivity:

$$\left.\begin{array}{l} \frac{k_{Thnf}}{k_{thnf}} = \frac{k_4+2k_{thnf}-2\Phi_4(k_{thnf}-k_4)}{k_4+2k_{thnf}+\Phi_4(k_{thnf}-k_4)},\ \frac{k_{thnf}}{k_{hnf}} = \frac{k_3+2k_{hnf}-2\Phi_3(k_{hnf}-k_3)}{k_3+2k_{hnf}+\Phi_3(k_{hnf}-k_3)}, \\ \frac{k_{hnf}}{k_{nf}} = \frac{k_2+2k_{nf}-2\Phi_2(k_{nf}-k_2)}{k_2+2k_{nf}+\Phi_2(k_{nf}-k_2)},\ \frac{k_{nf}}{k_f} = \frac{k_1+2k_{nf}-2\Phi_4(k_{nf}-k_4)}{k_1+2k_{nf}+\Phi_4(k_{nf}-k_4)}. \end{array}\right\} \tag{32}$$

5. Result and discussion

In this work, a mathematical model for the flow, heat transfer and mass transport properties of a tetra-hybrid nanofluid past a vertically moving rotating disk is analyzed by considering the von Karman flow model. A porous medium is introduced through the Darcy-Forchheimer resistance and a heat source or sink is introduced to analyze the thermal properties of the fluid. Also, homogeneous-heterogeneous chemical reactions are introduced to analyze the properties of species transfer. The considered effects have practical importance in many engineering applications. Similarity transformations are used to reduce the governing partial differential equations into a set of nonlinear ODEs. The equations obtained are solved numerically by using the RKF-45 method. A parametric study is carried out to analyze the impact of the considered parameters on the velocity, temperature and concentration profiles. The impact of the parameters is analyzed through graphs. Thermophysical properties of the tetra-hybrid nanoparticles and the base fluid are provided in Table 1.

Fig. 1 shows the behaviour of radial velocity $U(\eta)$ under varying values of Darcy-Forchheimer parameters. From the graph, it can be seen that $U(\eta)$ is inversely proportional to the Darcy-Forchheimer parameters that vary between 2 and 10. As per the von Karman flow principle, the disk movement induces radial flow of fluid while the Darcy-Forchheimer resistance acts against the disk movement. An increase in the value of the parameter implies increased porous media resistance, resulting in dissipation of radial

Table 1. The thermophysical values.

Properties	ρ	C_p	k
Water	997.1	4179	0.613
Al_2O_3	3970	765	40
Cu	8933	385	400
SiO_2	2200	754	1.4013
TiO_2	4250	686.2	8.9538

momentum. Fig. 2 shows the behaviour of $U(\eta)$ under varying values of porous media parameter K^*. When the parameter K^* is increased from 1 to 3, there is a drop in the value of the radial velocity, $U(\eta)$. When it comes to the von Karman flow in which the motion is created by the oscillation of a disk, the movement of the disk is responsible for the flow in the radial direction. An increase in K^* increases the drag on this radial flow by the porous media. This causes a reduction in the radial velocity of the fluid. The effect of the vertical reciprocation parameter S on the radial velocity $U(\eta)$ is shown in Fig. 3. It is seen that as the value of S changes from -0.3 to 0.5, the magnitude of the radial velocity increases gradually. In the case where S<0, due to downward reciprocation of the disk, the radial flow of the fluid is reduced, leading to low velocity magnitudes. As the value of S increases, the disk undergoes upward reciprocation and thus enhances the flow caused by the rotation and reciprocation of the disk. This leads to an increase in the radial momentum of the boundary layer fluid and hence the increase in the value of $U(\eta)$. Thus, the maximum and minimum values of the radial velocity are observed at 0.5 and -0.3, respectively. With the rise in the value of the F_1 from 2 to 10, there is a decrease in the tangential velocity $V(\eta)$ is shown in Fig. 4. The phenomenon can be explained by the increase in the resistance due to the porous medium towards the rotating flow created by the disk. In the von Karman setup, the disk creates tangential flow by transferring the angular momentum to the fluid. An increase in the Darcy-Forchheimer number will increase the drag and inertial forces inside the porous medium and hence the angular momentum is dissipated and the azimuthal fluid flow is restricted. This results in the reduction of tangential velocity with an increase in the Darcy-Forchheimer number. The influence of the parameter of porous medium K^* on the tangential velocity $V(\eta)$ is shown in Fig. 5. It can be seen that the tangential velocity decreases with the increase of K^* from 1 to 3. The phenomenon of the von Karman flow involves a situation where the rotational motion of the disk leads to an angular momentum being transferred to the surrounding fluid and gives rise to the tangential velocity. When K^* increases, the opposition offered by the porous medium to the motion of the fluid increases, thus opposing the rotational flow of the fluid. This, in turn, leads to a decrease in the angular momentum transferred to the fluid from the disk. Therefore, higher values of K^* lower the rotational motion of the fluid and lower the tangential velocity profile. Fig. 6 shows how the effect of the vertical reciprocation parameter S affects the tangential velocity $V(\eta)$. It is clear from the graph that tangential velocity increases with an increase in the value of S from -0.3 to 0.5. Vertical reciprocation of the disk will change the momentum distribution in the boundary layer and affect the interaction of the disk motion with the fluid. With an increase in the value of S, there is more influence of upward reciprocation of the disk on the tangential motion of the fluid, thereby increasing angular momentum exchange between the disk and fluid. As a result, the profile of tangential velocity increases, obtaining the maximum values at 0.5. The effect of the heat source/sink parameter on the temperature profile is presented in Fig. 7. It can be observed that as the heat source/sink parameter increases from 0.3 to 1.5, the temperature profile also increases. The physical interpretation for the increasing heat source/sink parameter is that it increases the heat generation in the fluid, leading to a higher amount of thermal energy in the fluid. The extra heat generation decreases the rate of dissipation of thermal energy from the fluid, thus causing the temperature profile to increase. Consequently, greater values of the heat source/sink parameter result in increased heat energy storage and hence an increase in the temperature profile. Fig. 8 shows the change in the temperature profile $\theta(\eta)$ for various values of the vertical reciprocation parameter S. There is a decrease in the $\theta(\eta)$ with an increase in the value of S from -0.1 to 0.1. The vertical reciprocation of the disk affects the convection process of energy transfer in the boundary layer. With the increase in the value of S, there is an increase in the upward motion of the disk and hence the energy transfer away from the disk region. As a result, the $\theta(\eta)$ falls with the increase in the value of S. Consequently, upward reciprocation of the disk will help improve thermal conductivity and decrease the temperature of the fluid. With the increase in the value of the homogeneous reaction parameter, K_1, from 0.1 to 1.3, there is a clear drop in the concentration distribution as shown in Fig. 9. As such, an increase in the value of K_1 indicates an increase in the rate of homogeneous reaction in the fluid. With a higher rate of reaction, there will be a faster rate of consumption of the species. This means that the concentration of the species will decrease within the fluid region. Increased consumption of the species results in the thinning of the concentration boundary layer and steeping of the concentration gradient close to the disk surface. Therefore, the concentration distribution reduces with an increase in K_1, which suggests that greater homogeneous chemical reactions result in mass transfer towards the reacting surface. The effect of the parameter S, which characterizes the vertical reciprocation, on the concentration profile $\chi(\eta)$ is depicted in Fig. 10. The concentration profile decreases as S varies from -0.3 to 0.3. As the S controls the vertical reciprocation of the disk, an increase in S from negative to positive values brings about change in the direction and strength of the motion from downward to upward reciprocation of the disk. The change in disk reciprocation affects the species transfer in the boundary layer. The increased upward reciprocation improves the convection of the species from the surface of the disk. The higher upward reciprocation strength increases the convective flow of the species from the disk surface, thus lowering its concentration in the fluid. Therefore, the concentration profile decreases with an increase in the value of S. The variation of the concentration profile under the impact of the Sc is shown in Fig. 11. The concentration profile rises with a rise in Sc from 1.2 to 2.4. Because Sc is negatively proportional to mass diffusivity, a high value of Sc shows that there will be low mass diffusion of molecules. This low mass diffusion causes less transfer of molecules, so they remain in the boundary layer in greater numbers; hence the concentration profile rises with rise in Sc.

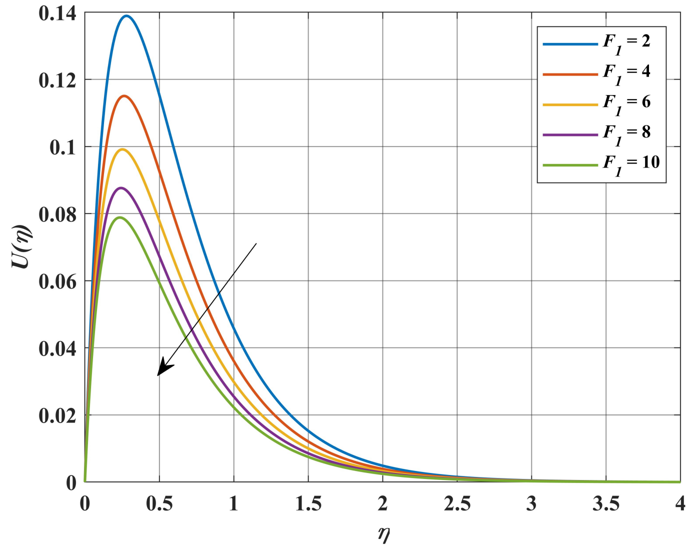

FIGURE 1. The impact of F_1 on $U(\eta)$.

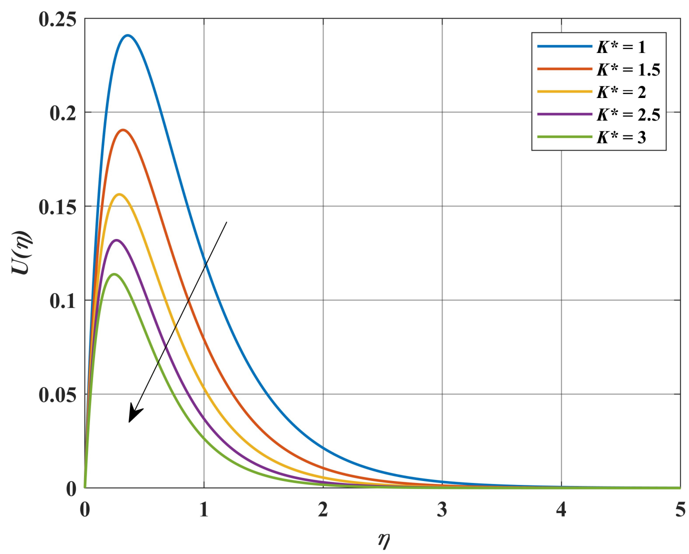

FIGURE 2. The impact of K^* on $U(\eta)$.

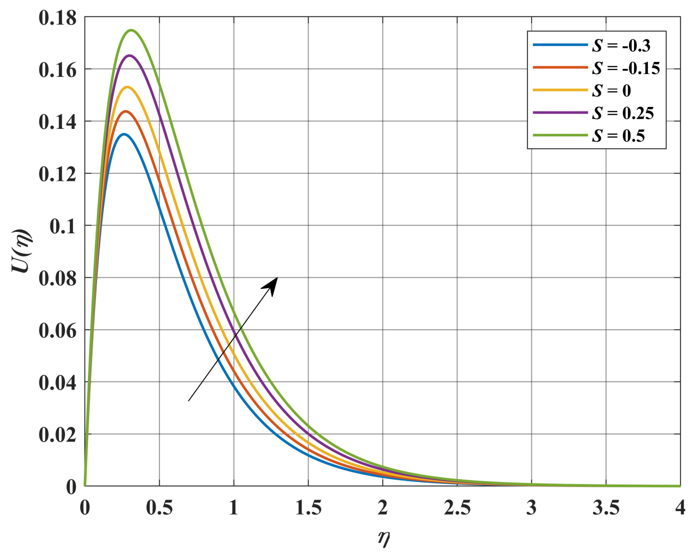

FIGURE 3. The impact of S on $U(\eta)$.

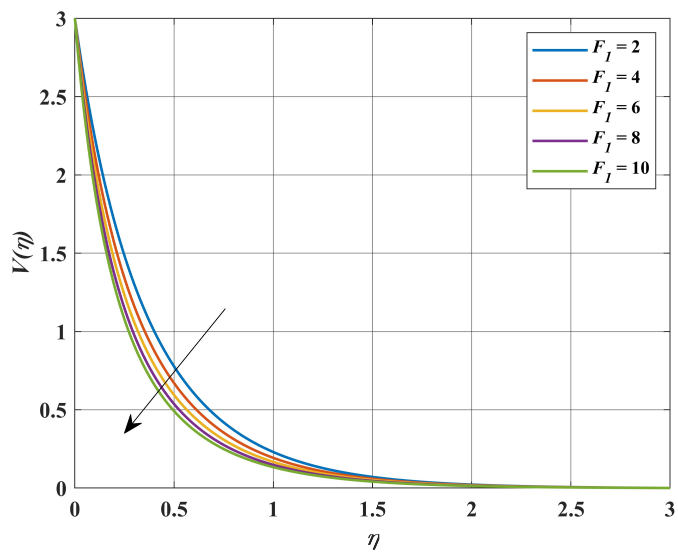

FIGURE 4. The impact of F_1 on $V(\eta)$.

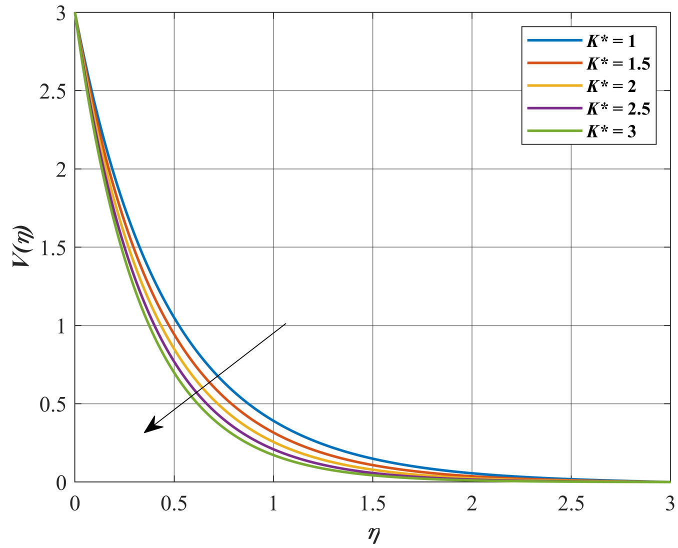

FIGURE 5. The impact of K^* on $V(\eta)$.

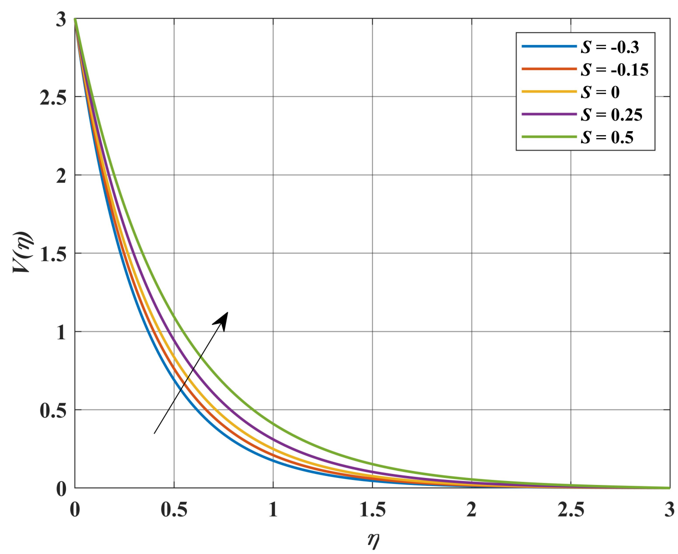

FIGURE 6. The impact of S on $V(\eta)$.

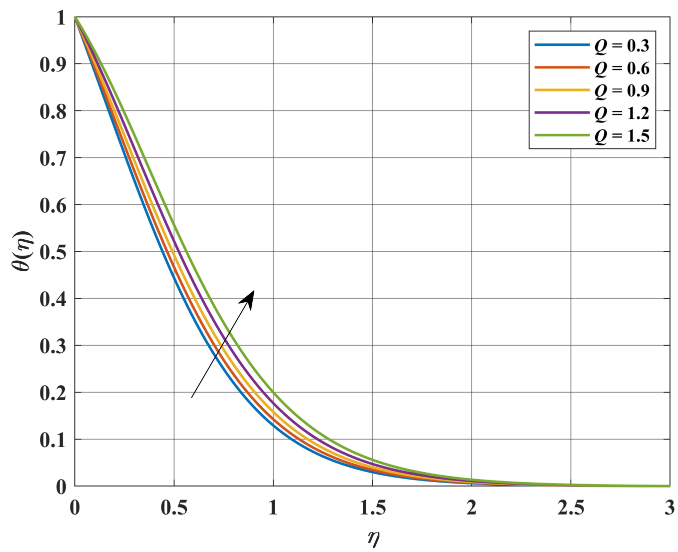

FIGURE 7. The impact of Q on $\theta(\eta)$.

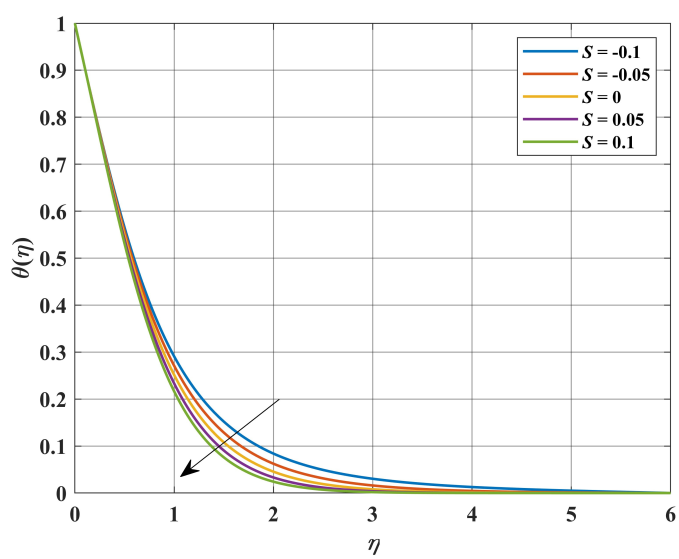

FIGURE 8. The impact of S on $\theta(\eta)$.

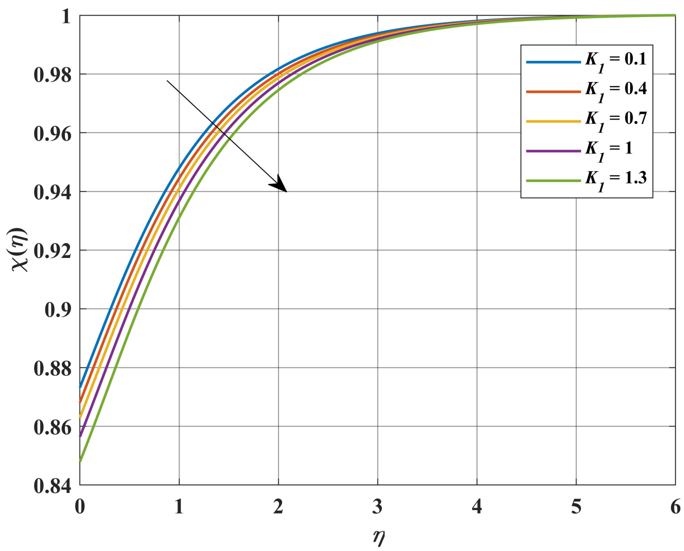

FIGURE 9. The impact of K_1 on $\chi(\eta)$.

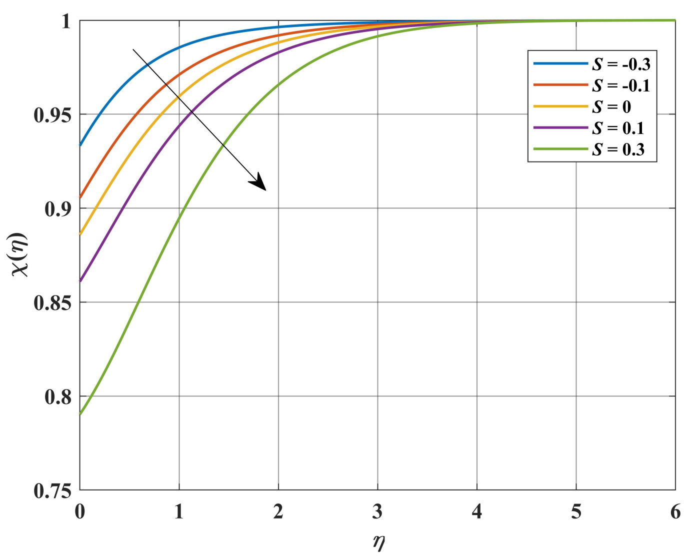

FIGURE 10. The impact of S on $\chi(\eta)$.

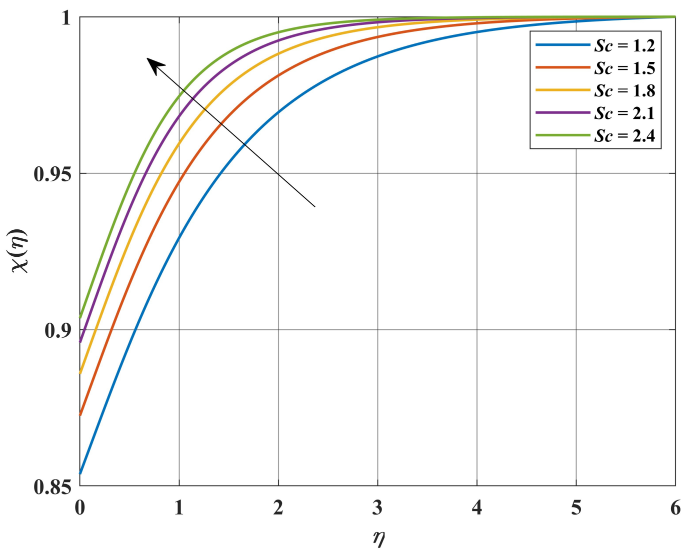

FIGURE 11. The impact of Sc on $\chi(\eta)$.

6. Response surface methodology

RSM is a statistical approach to analyze the relationship between multiple independent parameters and a response of interest. It uses mathematical modelling together with statistical techniques to understand how variations in the input parameters affect the response and identify the favourable working conditions. In this study, RSM is used to study the heat transfer properties of the flow under consideration with respect to the dimensionless governing parameters and temperature profile. Central composite design (CCD) is the design method that is used in this study since it enables the effects of selected parameters to be examined within a specific range by considering both linear and nonlinear behaviour. This design comprises factorial, axial, and centre points, which in total give enough data to create a second-order response surface model. The factorial points consist of combinations of the selected parameters at their coded lower and upper levels, while the axial points help to extend the design space. The centre points are included to check for the repeatability of the response and to determine the pure experimental or numerical error. In the current study, heat source/sink, reciprocating and porous media parameters are taken as the independent parameters, whereas the temperature profile is taken as the response parameter. A total of 20 numerical experiments are created based on the CCD and then analysed based on the governing mathematical model. The obtained numerical results are used to generate a quadratic regression equation that involves the main effects, interaction effects, and squared effects of the considered parameters. The significance and adequacy of the developed regression equation are checked based on the Analysis of Variance (ANOVA) by taking into account the P-values, F-values, coefficient of determination, and adjusted coefficient of determination. In addition to this, response surfaces and contour plots are plotted to show the effect of all the parameters on the response variable. Thus, the developed RSM model helps to determine the effect of all the governing parameters and their interactions on the heat transfer response, and a suitable statistical tool is provided to analyse and optimize the thermal behaviour of the system.

$$\begin{aligned}\theta(\eta) = \ & \Upsilon_1 + \Upsilon_2 A + \Upsilon_3 B + \Upsilon_4 C + \Upsilon_5 A * A + \Upsilon_6 B * B + \Upsilon_7 C * C + \Upsilon_8 A * B \\ & + \Upsilon_9 A * C + \Upsilon_{10}\ B * C\end{aligned}$$

In this case, Υ_i $(i = 1 - 10)$ is the set of coefficients that the quadratic response model determines after performing RSM. The coefficients represent the influence of the selected variables, the interactions between them, and the corresponding nonlinear effects on the heat transfer response. Thus, the final model gives the mathematical expression of how the factors influence the heat transfer response.

TABLE 2. Independent variables and their ranges.

Parameter	**Range**	**Level**		
		-1	**0**	**1**
Heat source/sink (Q)	0.3 to 1.5	0.3	0.9	1.5
Reciprocating parameter (S)	-0.3 to 0.1	-0.3	-0.1	0.1
Porous media parameter(K^*)	1 to 3	1	2	3

In the context of CCD, a second-order polynomial is derived to express the response in terms of the chosen operating parameters. The design matrix is generated through consideration of factorial combinations, centre points and axial points so that the region under study is adequately covered. While the factorial combinations help in studying the main effects and interaction effects of the control variables, the axial points give information about the nonlinearity of the response. The centre points additionally help in understanding the variation near the centre point of the design matrix. The chosen control variables along with their corresponding coded and real values are shown in Table 2. The regression equation thus helps in quantifying the effects of the control variables on heat transfer performance.

The statistical appropriateness of the developed heat transfer response model is analyzed using the ANOVA, with the corresponding analysis results presented in Table 3. In the framework of ANOVA analysis, the total variance of the response is split into the variances caused by the regression model and by the rest unexplained errors. Linear, interaction, and quadratic terms are analyzed separately with respect to their contribution to the calculated value of heat transfer. Statistical characteristics such as sum of squares, degrees of freedom, mean square, F-value and P-value are used to estimate the importance of the model and its components. The obtained statistical characteristics provide evidence of the appropriateness of the constructed polynomial in relation to the given numerical data. Based on this analysis, the constructed regression model is applicable for describing the variation of the heat transfer response in terms of the selected governing parameters.

$$\left.\begin{aligned}\theta(\eta) = \ & -5.15 + 1.389Q - 1.27S + 4.11K^* + 0.812Q * Q + 31.39S * S \\ & -0.840K^* * K^* + 5.68Q * S - 0.371Q * K^* + 2.63\ \mathrm{S} * K^*\end{aligned}\right\} \tag{33}$$

Model validation:

TABLE 3. ANOVA for $\theta(\eta)$.

Source	**DF**	**Seq SS**	**Contribution**	**Adj SS**	**Adj MS**	**F-Value**	**P-Value**
Model	9	2.00805	90.42%	2.00805	0.223116	10.49	0.001
Linear	3	0.60581	27.28%	0.84178	0.280592	13.19	0.001
Q	1	0.01768	0.80%	0.2945	0.294505	13.84	0.004
S	1	0.54552	24.56%	0.23245	0.232449	10.92	0.008
K^*	1	0.04261	1.92%	0.07584	0.07584	3.56	0.088
Square	3	1.01204	45.57%	1.10311	0.367704	17.28	0
$Q*Q$	1	0.07871	3.54%	0.01751	0.017512	0.82	0.386
$S*S$	1	0.764	34.40%	0.30449	0.304491	14.31	0.004
$K^* * K^*$	1	0.16933	7.62%	0.4659	0.465898	21.9	0.001
2-Way Interaction	3	0.3902	17.57%	0.3902	0.130065	6.11	0.012
$Q*S$	1	0.21616	9.73%	0.37485	0.37485	17.62	0.002
$Q*K^*$	1	0.0369	1.66%	0.03619	0.036187	1.7	0.221
$S*K^*$	1	0.13714	6.18%	0.13714	0.137137	6.45	0.029
Error	10	0.21278	9.58%	0.21278	0.021278		
Lack-of-Fit	1	0.21278	9.58%	0.21278	0.212777	*	*
Pure Error	9	0	0.00%	0	0		
Total	19	2.22083	100.00%				

The importance of the regression terms is established through the ANOVA test, where we use a 5% significance level. Specifically, the significance of the model term will be tested using P-values, where a model term will be important if its P-value is less than 0.05, meaning that its effect is statistically significant at the 95% confidence level. In this way, P-values for the linear, interaction, and quadratic terms in the response equation will be evaluated. If the terms are not significant based on the stated criterion, they will be dropped from the regression model as they do not have any importance in explaining the heat transfer response.

$$\left.\begin{array}{l}\theta(\eta) = \ -5.15 + 1.389Q - 1.27S + 4.11K^* + 31.39S*S - 0.840K^* * K^* \\ +5.68Q*S + 2.63\ \mathrm{S}*K^*\end{array}\right\} \tag{34}$$

TABLE 4. Summary of the model.

S	R^2	R^2(adj)	R^2(pred)
0.145869	90.42%	89.80%	87.31%

The R-square (R^2) and adjusted R-square (R^2) of the created RSM model are displayed in Table 4. The high values of these R-square (R^2) and adjusted R-square (R^2) imply that there is an excellent correlation between the predicted and actual heat transfer responses.

The residual plot for the temperature profile, as shown in Fig. 12, indicates the adequacy and accuracy of the regression model constructed. From the normal probability plot, it can be observed that the majority of the residuals fall on the reference line, hence indicating an approximately normal distribution. From the residual versus fitted plot, it can be observed that there is no pattern or funnel shape in the residual plot, but it is rather randomly distributed around zero. From the histogram, it can be observed that the majority of the residuals are centred around zero, while from the residual versus order plot, it can be observed that the residuals are randomly distributed without a pattern. The contour and surface plot for the temperature profile are illustrated in Fig. 13. These plots reveal the influence of Q, S and K^* together on the $\theta(\eta)$. From the plot of Q-K^*, an increase in Q significantly improves the temperature profile, while K^* exhibits nonlinearity where the maximum temperature is obtained at intermediate-higher K^*. For the plots of S-K^*, an increase in S causes an increase in $\theta(\eta)$, while the effect of K^* changes according to the value of S, implying that there is a notable interaction between the two variables. This is also evident from the plots of Q-S, where an increase in Q and S increases the temperature distribution; the maximum values of $\theta(\eta)$ are obtained in the region where Q and S are high and positive, respectively. Thus, the nonlinear plots show significant interactions among the parameters and indicate that Q, S and K^* interact together to affect the thermal behaviour of the system.

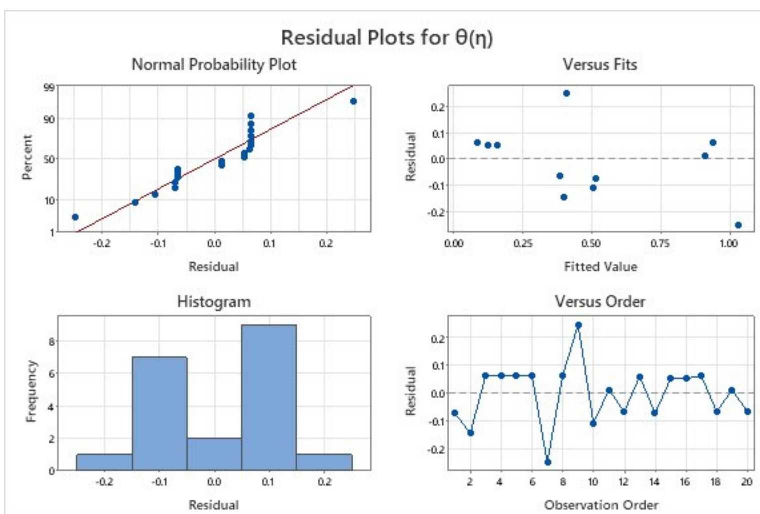

FIGURE 12. Residual plot for the temperature profile.

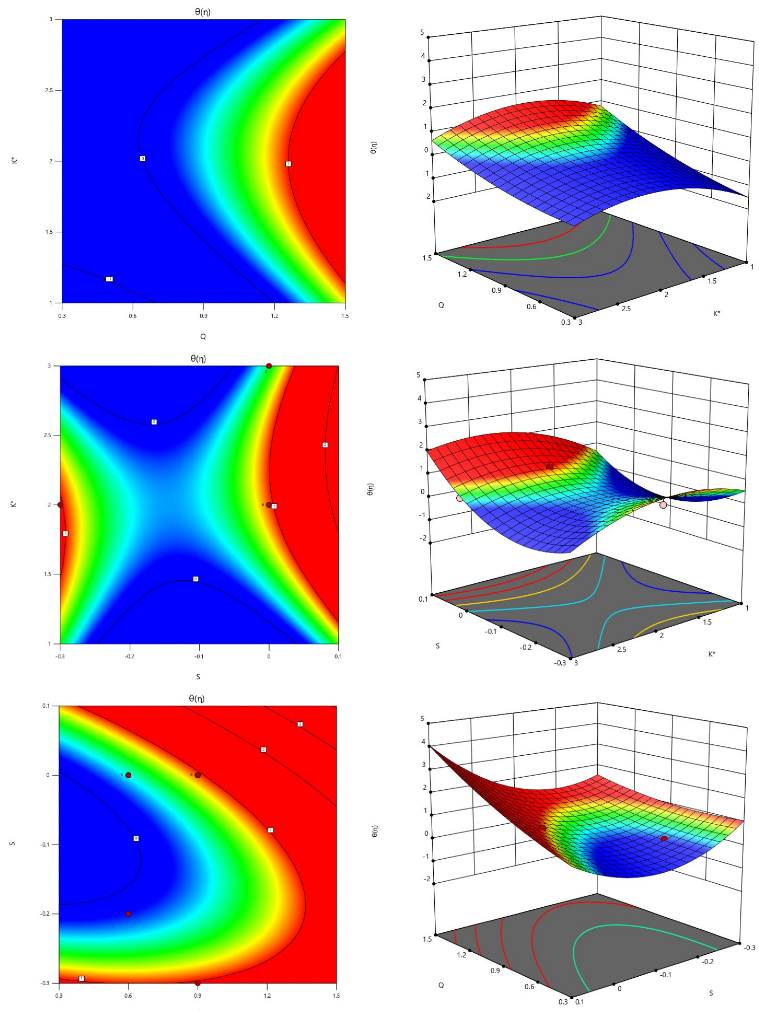

FIGURE 13. Contour and surface plot for the temperature profile.

7. Conclusion

The present study analyses the flow, heat and mass transfer attributes of a fluid due to a reciprocating disk in the von Karman flow setup. The impact of the following on the flow, thermal and concentration profiles is studied: vertical disk reciprocation, Darcy-Forchheimer drag, porous medium, heat source/sink, homogeneous-heterogeneous reaction and Schmidt number. The model nonlinear partial differential equations have been reduced to a set of ODEs via similarity transformation and solved numerically by the RKF-45 method. The important results of the study are as follows:

- The vertical reciprocation parameter greatly affects the transfer properties. With an increase in$S$, the values of the concentration and temperature profiles diminish while those of the tangential velocity increase, implying that vertical reciprocation alters the momentum, thermal, and mass transfer processes in the boundary layer.
- The increase in the Darcy-Forchheimer parameter leads to a decrease in the radial and tangential velocity profiles. The increased resistance offered by the porous medium impedes the fluid flow resulting from the rotating disk and thus dissipates the momentum.
- The porous medium parameter significantly affects the velocity profiles. Increase in K^*leads to a decrease in the radial and tangential velocities due to the increased resistance to the fluid flow in the porous medium.
- The effect of the heat source/sink parameter is to increase the temperature profile. It has the effect of increasing the amount of thermal energy supplied to the fluid, leading to accumulation of thermal energy and the temperature profile.
- The concentration distribution decreases with an increase in the K_1. The stronger reaction increases the rate of decay of the species, hence the concentration distribution.
- The concentration distribution increases with the increasing Schmidt number. Increasing Schmidt number corresponds to low mass diffusivity; therefore, species cannot diffuse easily, hence a high concentration profile.
- In general, the analysis shows that vertical reciprocation, resistance in the porous medium, heat generation, and chemical reaction are important tools to control momentum, heat, and mass transfer in reciprocating disk flow systems.
- The RSM model effectively describes the effect of interactions between the parameters that govern the behaviour, forming a good response surface model for the thermal behaviour.

Data Availability Statement

The findings of this work are based on theoretical analysis; no external data were required. Hence, all data generated or analysed during this study are included in this article.

References

1. O. A. Akbari, D. Toghraie and A. Karimipour, *Numerical Simulation of Heat Transfer and Turbulent Flow of Water Nanofluids Copper Oxide in Rectangular Microchannel with Semi-Attached Rib*, Advances in Mechanical Engineering, **8**(4) (2016), 1–25.
2. M. A. Bezerra, R. E. Santelli, E. P. Oliveira, L. S. Villar and L. A. Escaleira, *Response Surface Methodology (RSM) as a Tool for Optimization in Analytical Chemistry*, Talanta, 76(5) (2008), 965–-977.
3. Q-H. Deng, *Fluid Flow and Heat Transfer Characteristics of Natural Convection in Square Cavities Due to Discrete Source–Sink Pairs*, International Journal of Heat and Mass Transfer, **51**(25) (2008), 5949–-5957.
4. T. Hayat, M. Imtiaz and A. Alsaedi, *Effects of Homogeneous-Heterogeneous Reactions in Flow of Powell-Eyring Fluid*, Journal of Central South University, **22**(8) (2015), 3211–-3216.
5. Y. Hirata, T. Dote, T. Yoshioka, Y. Komoda and Y. Inoue, *Performance of Chaotic Mixing Caused by Reciprocating a Disk in a Cylindrical Vessel*, Chemical Engineering Research and Design, **85**(5) (2007), 576–-582.

6. P. K. Kameswaran, S. Shaw, P. Sibanda and P. V. S. N. Murthy, *Homogeneous–Heterogeneous Reactions in a Nanofluid Flow Due to a Porous Stretching Sheet*, International Journal of Heat and Mass Transfer, **57**(2) (2013), 465–-472.
7. A. I. Khuri and S. Mukhopadhyay, *Response Surface Methodology*, WIREs Computational Statistics, **2**(2) (2010), 128–-149.
8. Y. Komoda, Y. Inoue, and Y. Hirata, *Mixing Performance by Reciprocating Disk in Cylindrical Vessel*, Journal of Chemical Engineering of Japan, **33**(6) (2000), 879–-885.
9. Y. Komoda, Y. Inoue, and Y. Hirata, *Characteristics of Laminar Flow Induced by Reciprocating Disk in Cylindrical Vessel*, Journal of Chemical Engineering of Japan, **34**(7) (2001), 919-–928.
10. H. A. Mohammed, G. Bhaskaran, N. H. Shuaib and R. Saidur, *Heat Transfer and Fluid Flow Characteristics in Microchannels Heat Exchanger Using Nanofluids: A Review*, Renewable and Sustainable Energy Reviews, **15**(3) (2011), 1502–-1512.
11. D. Pal, *Combined Effects of Non-Uniform Heat Source/Sink and Thermal Radiation on Heat Transfer over an Unsteady Stretching Permeable Surface*, Communications in Nonlinear Science and Numerical Simulation, **16**(4) (2011), 1890–-1904.
12. M. Qasim, *Heat and Mass Transfer in a Jeffrey Fluid over a Stretching Sheet with Heat Source/Sink*, Alexandria Engineering Journal, **52**(4) (2013), 571–-575.
13. S. Shaw, P. K. Kameswaran, and P. Sibanda, *Homogeneous-Heterogeneous Reactions in Micropolar Fluid Flow from a Permeable Stretching or Shrinking Sheet in a Porous Medium*, Boundary Value Problems, **2013**(1) (2013), Article Number: 77, 10 Pages.
14. M. Sheikholeslami, M. Hatami and D. D. Ganji, *Nanofluid Flow and Heat Transfer in a Rotating System in the Presence of a Magnetic Field*, Journal of Molecular Liquids, **190** (2014): 112–-120.
15. T. K. Trinh, and L. S. Kang, *Application of Response Surface Method as an Experimental Design to Optimize Coagulation Tests*, Environmental Engineering Research, **15**(2) (2010), 63-–70.

S. Prasanna Rani: Department of Mathematics, ABV Government Degree College, Jangaon-506 167, Telangana, India.
Email address: prasannaradhakrishna28@gmail.com